JACS
JOURNAL OF THE AMERICAN CHEMICAL SOCIETY

Communication

pubs.acs.org/JACS

High-Performance Solution-Processed Solar Cells and Ambipolar Behavior in Organic Field-Effect Transistors with Thienyl-BODIPY Scaffoldings

Thomas Bura,[†] Nicolas Leclerc,[‡] Sadiara Fall,[§] Patrick Lévêque,[§] Thomas Heiser,[§] Pascal Retailleau,[⊥] Sandra Rihn,[†] Antoine Mirloup,[†] and Raymond Ziessel*[,†]

[†]Laboratoire de Chimie Moléculaire et Spectroscopies Avancées LCOSA, Ecole Européenne de Chimie, Polymères et Matériaux, UMR 7515 associé au CNRS, 25 rue Becquerel, 67087 Strasbourg Cedex 02, France

[‡]Laboratoire d'Ingénierie des Polymères pour les Hautes Technologies, Université de Strasbourg, Ecole Européenne de Chimie, Polymères et Matériaux, 25 rue Becquerel, 67087 Strasbourg, France

[§]Institut d'Electronique du Solide et des Systèmes, Université de Strasbourg-CNRS, 23 rue du Loess, 67037 Strasbourg, France

[⊥]Centre de Recherche de Gif, Institut de Chimie des Substances Naturelles, CNRS, Bât. 27-1 avenue de la Terrasse, 91198 Gif-sur-Yvette Cedex, France

Supporting Information

ABSTRACT: Green-absorbing dipyrromethene dyes engineered from bis-vinyl-thienyl modules are planar molecules, exhibiting strong absorption in the 713−724 nm range and displaying comparable electron and hole mobilities in thin films (maximum value 1×10^{-3} $cm^2/(V{\cdot}s)$). Bulk heterojunction solar cells assembled with these dyes and a fullerene derivative ($PC_{61}BM$) at a low ratio give a power conversion efficiency as high as 4.7%, with short-circuit current values of 14.2 mA/cm^2, open-circuit voltage of 0.7 V, and a broad external quantum efficiency ranging from 350 to 920 nm with a maximum value of 60%.

Plastic electronic devices provide prototypes for many electronic applications, including information technology, renewable energy harvesting, life sciences, and biomedicine ("bioships").[1] In this regard, organic field-effect transistors (OFETs)[2] and solution-processed polymer bulk-heterojunction (BHJ)[3] solar cells have been widely investigated, with impressive successes concerning ambipolar charge transport and power conversion efficiency (PCE), respectively. In this rapidly advancing field, small conjugated organic molecules, molecular assemblies, and gelators[4] are very attractive candidates, as they can be provided pure and in large amounts through reproducible and well-established synthetic protocols. Thin films with good characteristics can easily be produced by spin-coating, casting, or printing under ambient conditions. Spectacular results have been obtained with various chemical frameworks,[3c,d] of which oligothiophenes,[5] diketopyrrolopyrrole (DPP),[6] squaraine,[7] hexabenzo-coronenes,[8] merocyanine,[9] donor−acceptor oxoindane,[10] and thiadiazolo-bithienyl dyes[11] lie at the forefront owing to their high PCEs, reaching about 7% in the best case. Boron dipyrromethene (BODIPY) dyes[12] are characterized by outstanding chemical and photochemical stabilities, redox activity, and optical features that can easily be tailored by chemical transformation, allowing them to be used in BHJ solar cells.[13] To be efficient in such devices, the dyes must fulfill at least the following requirements: (i) strong optical absorption in the wavelength range from 500 to 900 nm; (ii) a sufficiently large energy difference between the LUMO of the dye and the LUMO of the acceptor (such as PCBM); (iii) a deep HOMO of the dye to maximize the open-circuit voltage (V_{OC}); (iv) a near-planar molecular structure to favor local organization and a good charge carrier mobility in the film to maximize the short-circuit current (J_{SC}) and fill factor (FF); (v) adequate solubilizing side chains to ensure good filmability when blended with PCBM; and finally (vi) the dyes must be robust and easily prepared.

Planar BODIPYs engineered from vinyl-thiophene modules and with various solubilizing chains at the periphery are unknown but accessible with dedicated protocols.[14] Such dyes possess most of the attributes listed above to produce high-performance solar cells.

It is now well established that solubilizing side chains deeply impact organic materials' semiconducting properties.[15,16] In the present work, we have synthesized a new series of thienyl-BODIPY dyes ($\mathbf{TB}_n$ in Chart 1) and investigated their physical and optoelectronic properties as well as their performances as active materials in both field-effect transistors and organic solar cells, with a special focus on the influence of the solubilizing chains. The dyes were prepared by Knovenagel condensation of the aldehyde $\mathbf{T}_n$ with a tetramethyl BODIPY derivative under established conditions.[17]

Differential scanning calorimetry (DSC) measurements indicate that $\mathbf{TB}_2$ is a semicrystalline material with reproducible melting and crystallization thermal transitions (mp = 245 °C and cp = 220 °C). The other molecules remain amorphous, showing a melting transition only during the first heating ramp (see SI).

In order to investigate the molecular structure along with the packing structure, we grew single crystals of $\mathbf{TB}_2$. X-ray

Received: August 7, 2012
Published: October 5, 2012

   dx.doi.org/10.1021/ja3072513 | J. Am. Chem. Soc. 2012, 134, 17404−17407

Chart 1. Thiophene-BODIPYs (TB_n) Studied Herein

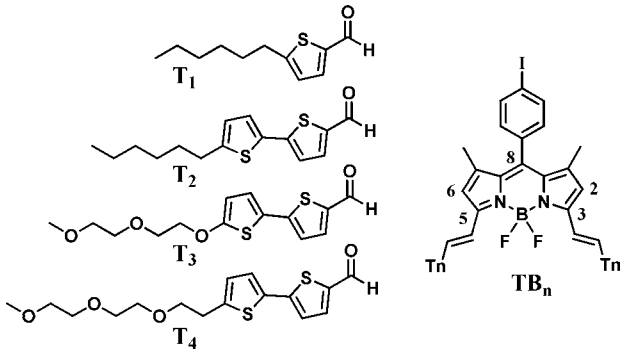

diffraction establishes that the TB_2 framework substituents are essentially coplanar with the near-planar BODIPY core (maximum deviation from the mean least-squares plane is 0.17(1) Å for the boron atom; Figure 1). There is a slight

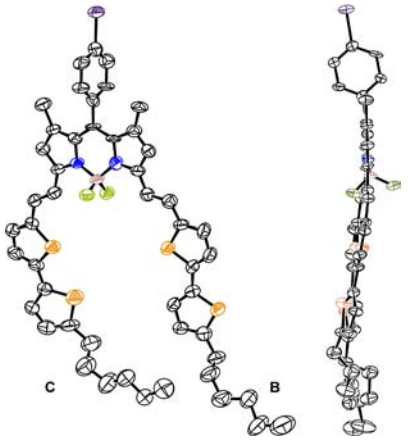

Figure 1. ORTEP view of compound TB_2. Displacement ellipsoids are drawn at the 50% probability level, and H atoms are shown as small spheres of arbitrary radii. On the right is shown a perpendicular view along the BODIPY axis, highlighting the planar structure and the perpendicular iodophenyl fragment.

curvature of the overall structure with respect to the BODIPY core. The orthogonally attached (83.8°) iodophenyl group (∠B1−C8−I1 > 173.3°) on one side and the mean plane constituted by the two vinyl-bithiophene arms (B and C, dihedral angle 9.3°) on the other lead to a distortion that is partially compensated by bending of the hexyl chains. Interestingly, the inner thiophene groups are head-to-head, whereas the outer thiophenes are head-to-tail, with dihedral angles between the two pairs of thiophene rings of 7.8° (B) and 17.1° (C). Arm C is curved toward arm B, with the shortest contact being C16C···C11B = 3.83 Å. The two arms define an ellipsoidal area of approximately 10 × 7 $Å^2$, into which protrudes the iodo atom of the iodophenyl substituent of a neighboring molecule along the *b* axis so as to make a short contact to F (I···F = 3.13 Å) (Figure 2). These interactions cross-link the (3 1 3) planes in which the inversion-related molecules lie in chains with the double-thiophene arms side by side in the [1 0 −1] direction, producing zipper-like motifs of the iodobenzene groups. $\pi-\pi$ stacking interactions between layers involve overlap of both thiophene-vinylpyrrole moieties of a molecule at general position *x*, *y*, *z* with the equivalent inverted moiety from molecules at positions $1-x$, $3-y$, $1-z$

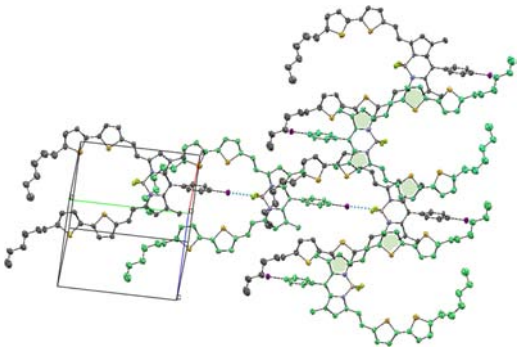

Figure 2. Packing view down the *ac* direction. Molecules with the same color code lie within the same layer. Dotted cyan lines indicate I···F interactions. Green-colored rings indicate $\pi-\pi$ stacking between molecules at *x*, *y*, *z* and in an adjacent layer.

and $2-x$, $3-y$, $-z$. The centroid−centroid distances involving a pyrrole group and a thiophene group range from 3.710(4) to 3.954(5) Å.

The TB_{2-4} dyes in THF display two intense absorption peaks in the 430−450 and 560−750 nm ranges with extinction coefficients of about 100 000 $M^{-1}cm^{-1}$ (Figure 3 and Table

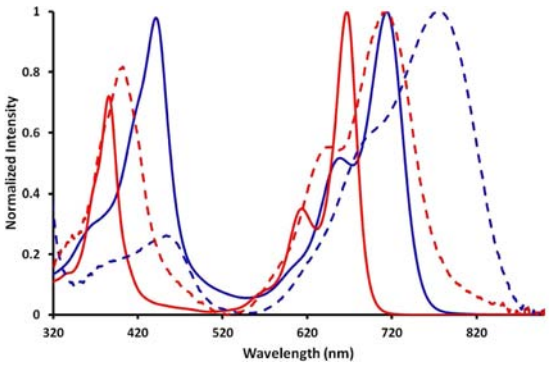

Figure 3. Absorption of TB_1 (red trace) and TB_2 (blue trace) in THF solution and thin films (dashed traces).

S1). The more energetic transition is due to the styryl residues while the less energetic is the $S_0 \rightarrow S_1$ of the indacene unit with a clear vibronic structure ($\Delta\nu$ = 1330 cm^{-1}). In contrast, the absorption of dye TB_1 is blue-shifted by 47 nm. This could be explained by the less conjugated styryl monothiophene arms with regard to the bithiophene styryl units of TB_{2-4}. All TB_n dyes exhibit fluorescence in the near-infrared (Table S1). In all cases the excitation spectra perfectly match the absorption spectra, excluding the presence of aggregates. In thin films (thickness of about 110 nm) the absorption is enlarged, peaking at 720 and 780 nm respectively for TB_1 and TB_2 (Figure 3) and indicating an optical band gap of about 1.60 and 1.45 eV, respectively. Cyclic voltammetry was used to determine the HOMO/LUMO levels of the dyes in solution after calibrating them with respect to $PC_{61}BM$ and ferrocene. The TB_2 dye displays two reversible oxidation waves at about +0.64 and +0.82 V respectively, assigned in light of previous results to the BODIPY radical cation and dication. The two reversible reduction waves at about −0.89 and −1.62 V are assigned to the BODIPY radical anion and dianion (Figure 4, Table S2).[18]

The bis-thienyl module is not electroactive within the +1.40 to −1.40 V window. $PC_{61}BM$ and ferrocene were used as

dx.doi.org/10.1021/ja3072513 | J. Am. Chem. Soc. 2012, 134, 17404−17407

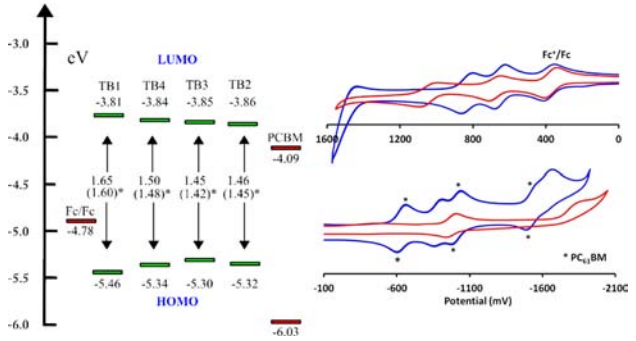

Figure 4. (Left) Position of the frontier molecular orbital energies versus $PC_{61}BM$ and ferrocene for all dyes. The electrochemical gaps were determined in solution and the optical gaps on thin films are given in parentheses. (Right) Cyclic voltammetry of $\mathbf{TB_2}$, ferrocene, and $PC_{61}BM$: (top) cathodic window; (bottom) anodic window.

internal references, enabling establishment of the frontier molecular orbital energies for each dye with respect to the electron acceptor ($PC_{61}BM$) (Figure 4). The electrochemical gap calculated from the HOMO/LUMO ranges from 1.45 to 1.50 eV for $\mathbf{TB_{2-4}}$ and is equal to 1.65 eV for $\mathbf{TB_1}$, which matches fairly well with the optical gap determined in the thin film. The energy data indicate that all four dyes are suitable candidates to be used as electron donors when blended with $PC_{61}BM$ in BHJ solar cells. Importantly, the low-lying HOMO level is desirable for a high V_{oc}, while the energy offset of the dye LUMO and $PC_{61}BM$ LUMO is about 0.23 V, a value close to the ideal case.[16]

Charge carrier mobilities in the dyes were measured by using them as a semiconductor layer in standard bottom-contact OFETs. The experimental procedure used for the device elaboration and the mobility measurements are given in Table S3.

$\mathbf{TB_2}$ exhibited rather distinctive behavior in comparison to the other molecules. Indeed, an unexpected ambipolar character was observed together with relatively high and comparable electron and hole mobilities (Figure 5).

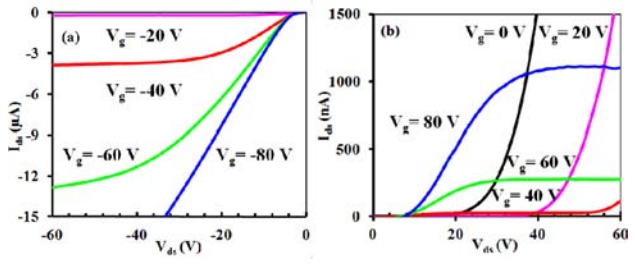

Figure 5. $I_{ds}-V_{ds}$ plots characteristic for $\mathbf{TB_2}$ OFETs obtained for (a) holes and (b) electrons.

The other molecules exhibit only hole transport with significantly lower mobilities (1×10^{-4} $cm^2/(V{\cdot}s)$ for $\mathbf{TB_1}$, 1×10^{-8} $cm^2/(V{\cdot}s)$ for $\mathbf{TB_3}$, and 6×10^{-7} $cm^2/(V{\cdot}s)$ for $\mathbf{TB_4}$). Similar OFET measurements on $\mathbf{TB_2}$ gave hole and electron mobility in the 1×10^{-3} $cm^2/(V{\cdot}s)$ range, i.e., up to 5 orders of magnitude higher hole mobility with respect to $\mathbf{TB_3}$. These high mobility values are in line with the high propensity of this planar dye to organize in three dimensions with strong intermolecular interactions (I···F and $\pi-\pi$-stacking) favoring short distances between neighboring molecules in the solid state (Figure 2). This behavior opens the way to a wide range of applications such as electroluminescent OFETs and complementary metal oxide semiconductor (CMOS) devices and circuits.[20]

BHJ devices were investigated using the dyes, blended with $PC_{61}BM$, as the active layer. The standard device structure was glass/ITO/PEDOT:PSS(~40 nm)/dyes:$PC_{61}BM$/Al-(~120 nm). Various dye:$PC_{61}BM$ mass ratios and different film thicknesses have been explored. The device current versus voltage ($J-V$) curves have been measured in darkness and under solar light (AM1.5G solar simulator at 100 mW/cm^2) on 9 mm^2 diodes. More details on the elaboration and characterization procedures can be found in the SI. The photovoltaic parameters achieved for cells with an optimized dye:$PC_{61}BM$ ratio are shown in Figure 6 for $\mathbf{TB_2}$ and are summarized in Table 1.

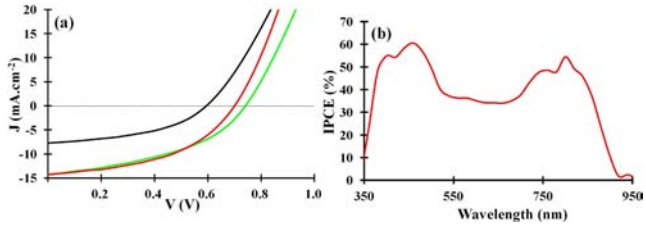

Figure 6. (a) $J-V$ characteristics for the best $\mathbf{TB_2}$ photovoltaic cells with an active layer obtained from chloroform solution with a $\mathbf{TB_2}$ concentration of 5 mg/mL (black) and from chlorobenzene solutions with a $\mathbf{TB_2}$ concentration of 40 mg/mL and an Al cathode (green) or a Ca/Al cathode (red) under standard AM1.5G (100 mW/cm^2) irradiation. (b) IPCE spectrum corresponding to the best $\mathbf{TB_2}$ photovoltaic cells with an active layer obtained from chlorobenzene solutions with a $\mathbf{TB_2}$ concentration of 40 mg/mL and an Al cathode.

Table 1. Photovoltaic Characteristics for Solution-Processed BHJ Solar Cells under Optimized Conditions

dye	TB:PCBM	V_{oc} (V)	J_{sc} (mA/cm^2)	FF (%)	PCE (%)	annealing temp, time (°C, min)
$\mathbf{TB_1}$	1:2[a]	0.76	5.84	31	1.4	70, 20
$\mathbf{TB_2}$	1:0.8[b]	0.74	14.2	43	4.5	100, 10
$\mathbf{TB_2}$	1:0.5[c]	0.7	14.3	47	4.7	120, 20
$\mathbf{TB_3}$	1:2[a]	0.56	5.1	30	0.9	–
$\mathbf{TB_4}$	1:1[a]	0.55	8.5	32	1.5	80, 20

[a]From chloroform solutions with a $\mathbf{TB_n}$ concentration of 5 mg/mL (active layer thickness: 110 ± 10 nm). [b]From chlorobenzene solutions with a $\mathbf{TB_n}$ concentration of 40 mg/mL and an Al cathode (active layer thickness: 165 ± 10 nm). [c]From chlorobenzene solutions with a $\mathbf{TB_n}$ concentration of 40 mg/mL and a Ca(20 nm)/Al(120 nm) bilayer cathode (active layer thickness: 165 ± 10 nm).

$\mathbf{TB_1}$ exhibits a higher V_{oc} value, in agreement with a deeper lying HOMO level.[19] On the other hand, $\mathbf{TB_2}$-based devices shows FF values about 45%. Moreover, increasing the $\mathbf{TB_2}$:$PC_{61}BM$ device thickness improves the device performances, while the opposite occurs for the other dyes (see SI). With a J_{sc} of 14.2 mA/cm^2 and a V_{oc} as high as 0.74 V, a PCE of up to 4.5% could be reached. The J_{sc} value is consistent with the broad external quantum efficiency (EQE), which reaches a maximum value of 60% and expands from 350 to 920 nm while remaining above 40% at the absorption minimum close to 550 nm (Figures 3 and 6b). The remarkably high J_{sc} value is a consequence of both the $\mathbf{TB_2}$ band gap (1.45 eV), which matches the optimum value predicted by Shockley and

dx.doi.org/10.1021/ja3072513 | J. Am. Chem. Soc. 2012, 134, 17404–17407

Queisser for a single-junction solar cell,[21] and the large extinction coefficient of BODIPY dyes, which allows significant photon absorption even within the low absorption region. Additionally, the relatively high V_{oc} is a result of the low-lying HOMO level of the dye, as may be expected from the previously established correlation between the donor-HOMO/acceptor-LUMO offset and V_{oc}.[19] The significantly lower performances achieved when using **TB$_3$** or **TB$_4$** dyes, whose frontier orbital energy levels are similar to those of **TB$_2$**, are most likely due to the much lower hole mobilities, causing inefficient charge separation and collection. The rapid drop in device performances with increasing active layer thickness corroborates this conclusion. An unfavorable morphology of the dye:PC$_{61}$BM blends may also contribute to the poor device operation in these cases. Atomic force microscopy measurements performed on annealed blends (Figure S34) show that **TB$_1$**-, **TB$_3$**-, and **TB$_4$**-based blends exhibit an amorphous surface morphology without noticeable macrophase separation. On the other hand, **TB$_2$**-based annealed blends show clear lamella-like features. These observations highlight again the very specific behavior of **TB$_2$**. It is likely that the enhanced molecular ordering of **TB$_2$** is at the origin of the observed relatively high charge carrier mobilities and thereby contributes to the good device performances.

In order to increase the FF of the **TB$_2$** devices, we reduced the **TB$_2$**:PC$_{61}$BM weight ratio in agreement with complementary OFET experiments (Figure S43) and added a 20 nm thick Ca layer to improve the electrical contact to the cathode. Together, the bilayer cathode and the lower 1:0.5 **TB$_2$**:PC$_{61}$BM content allowed us to slightly increase the FF and achieve a PCE of 4.7%. It is very likely that further optimization of the metal/organic interfaces and layer thicknesses may allow us to enhance the FF and EQE values and improve the PCE further.

In summary, we have designed new green-absorbing dyes based on thienyl-BODIPY frameworks, which provide a maximum power conversion efficiency of 4.7% in solution-processed BHJ solar cells. The planar bis-thienyl-BODIPY derivatives favor short contact distances between neighboring molecules in the solid state and exhibit high charge mobility and an ambipolar behavior. Challenging studies are now in progress to collect more efficiently the photons in the 500−620 nm range in order to further improve the device efficiency.

■ ASSOCIATED CONTENT

Supporting Information

General methods, synthetic experimental part, absorption and fluorescence spectra, traces NMR spectra, DSC traces, electrochemical data, devices preparation, and mobilities. This material is available free of charge via the Internet at http://pubs.acs.org.

■ AUTHOR INFORMATION

Corresponding Author

ziessel@unistra.fr

Notes

The authors declare no competing financial interest.

■ ACKNOWLEDGMENTS

We thank the Centre National de la Recherche Scientifique (CNRS) for financial support of this work. N. Zimmermann is kindly acknowledged for is help in photovoltaic devices elaboration.

■ REFERENCES

(1) *Handbook of Organic Electronics and Photonics*, Vols. 1−3; Nalwa, H. S., Ed.; American Scientific Publishers: Los Angeles, CA, 2008.
(2) Chua, L. L.; Zumseil, J.; Chang, J. F.; Ou, E. C. W.; Ho, P. K. H.; Sirringhaus, H.; Richard, R. H. *Nature* **2005**, *434*, 194−199.
(3) (a) Boudreault, P.-L. T.; Najari, A.; Leclerc, M. *Chem. Mater.* **2011**, *23*, 456−469. (b) Walker, B.; Kim, C.; Nguyen, T.-Q. *Chem. Mater.* **2011**, *23*, 470−482. (c) Beaujuge, P. M.; Fréchet, J. M. J. *J. Am. Chem. Soc.* **2011**, *133*, 20009−20029. (d) Mishra, A.; Bäuerle, P. *Angew. Chem., Int. Ed.* **2012**, *51*, 2020−2067. (e) Zhou, H.; Yang, L.; You, W. *Macromolecules* **2012**, *45*, 607−632.
(4) (a) Prasanthkumar, S.; Saeki, A.; Seki, S.; Ajayaghosh, A. *J. Am. Chem. Soc.* **2010**, *132*, 8866−8867. (b) Babu, S. S.; Prasanthkumar, S.; Ajayaghosh, A. *Angew. Chem., Int. Ed.* **2012**, *51*, 1766−1776.
(5) Fitzner, R.; Reinold, E.; Mishra, A.; Mena-Osteritz; Ziehlke, H.; Körner, C.; Leo, K.; Riede, M.; Weil, M.; Tsaryova, O.; Weiss, A.; Uhrich, C.; Pfeiffer, M.; Bäuerle, P. *Adv. Funct. Mater.* **2011**, *21*, 897−910.
(6) Walker, B.; Tamayo, A. B.; Dang, X.-D.; Zalar, P.; Seo, J. H.; Garcia, A.; Tantiwiwat, M.; Nguyen, T.-Q. *Adv. Funct. Mater.* **2009**, *19*, 3063−3069.
(7) (a) Wei, G.; Wang, S.; Sun, K.; Thompson, M. E.; Forrest, S. R. *Adv. Eng. Mater.* **2011**, *2*, 184−187. (b) Ajayaghosh, A. *Acc. Chem. Res.* **2005**, *38*, 449−459.
(8) Wong, W. W. H.; Singh, T. B.; Vak, D.; Pisula, W.; Yan, C.; Feng, X.; Williams, E. L.; Chan, K. L.; Mao, Q.; Jones, D. J.; Ma, C.-Q.; Müllen, K.; Baüerle, P.; Holmes, A. B. *Adv. Funct. Mater.* **2010**, *20*, 927−938.
(9) Kronenberg, N. M.; Deppisch, M.; Würthner, F.; Ladermann, H. W. A.; Deing, K.; Meerholz, K. *Chem. Commun.* **2008**, 6489−6491.
(10) Bürckstümmer, H.; Tulyakova, E. V.; Deppisch, M.; Lenze, M. R.; Kronenberg, N. M.; Gsänger, M.; Stolte, M.; Meerholz, K.; Würthner, F *Angew. Chem., Int. Ed.* **2011**, *4506*, 11628−11632.
(11) Sun, Y.; Welch, G. C.; Leong, W. L.; Takacs, C. J.; Bazan, G. C.; Heeger, A. J. *Nat. Mater.* **2011**, *11*, 44−48.
(12) (a) Ziessel, R.; Ulrich, G.; Harriman, A. *New J. Chem.* **2007**, *31*, 496−501. (b) Ulrich, G.; Ziessel, R.; Harriman, A. *Angew. Chem., Int. Ed.* **2008**, *47*, 1184−1201.
(13) (a) Rousseau, T.; Cravino, A.; Bura, T.; Ulrich, G.; Ziessel, R.; Roncali, J. *Chem. Commun.* **2009**, 1673−1675. (b) Lin, H.-Y.; Huang, W.-C.; Chou, H.-H.; Hsu, C.-Y.; Lin, J. T.; Lin, H. W. *Chem. Commun.* **2012**, *48*, 8913−8915.
(14) (a) Benniston, A. C.; Copley, G.; Harriman, A.; Ryan, R. *J. Mater. Chem.* **2011**, *21*, 2601−2608. (b) Chen, Y.; Zhao, J.; Guo, H.; Xie, L. *J. Org. Chem.* **2012**, *77*, 2192−2206. (c) Zhang, X.; Yu, H.; Xiao, Y. *J. Org. Chem.* **2012**, *77*, 669−673 and references therein.
(15) (a) Biniek, L.; Fall, S.; Chochos, C. L.; Anokhin, D. V.; Ivanov, D. A.; Leclerc, N.; Lévêque, P.; Heiser, T. *Macromolecules* **2010**, *43*, 9779−9786. (b) Fall, S.; Biniek, L.; Leclerc, N.; Lévêque, P.; Heiser, T. *Appl. Phys. Lett.* **2012**, *101*, 123301-1−123301-4.
(16) Chu, T. Y.; Lu, J.; Beaupré, S.; Zhang, Y.; Pouliot, J. R.; Zhou, J.; Najari, A.; Leclerc, M.; Tao, Y. *Adv. Funct. Mater.* **2012**, *22*, 2345−2351.
(17) Ziessel, R.; Bura, T.; Olivier, J.-H. *Synlett* **2010**, 2304−2310.
(18) Ziessel, R.; Bonardi, L.; Retailleau, P.; Ulrich, G. *J. Org. Chem.* **2006**, *71*, 3093−3102.
(19) Dennler, G.; Scharber, M. C.; Brabec, C. *J. Adv. Mater.* **2009**, *21*, 1323−1338.
(20) See, for instance: Anthopoulos, T. D.; Setayesh, S.; Smits, E.; Cölle, M.; Cantore, E.; de Boer, B.; Blom, P. W. M.; de Leeuw, D. M. *Adv. Mater.* **2006**, *18*, 1900−1904.
(21) Shockley, W.; Queisser, H. J. *J. Appl. Phys.* **1961**, *32*, 510−519.